# Tuning of microcapsule adhesion by varying the capsule-wall thickness

Nils Elsner, Frédéric Dubreuil, and Andreas Fery*
*Department of Interfaces, Max Planck Institute of Colloids and Interfaces, 14424 Potsdam, Germany*
(Received 2 July 2003; published 24 March 2004)

The adhesion area and topology of spherical hollow polyelectrolyte shells adhering to flat glass or polyelectrolyte-covered glass surfaces are studied. Strong adhesion is found for anionic poly(sodium 4-styrenesulfonate)-terminated shells on cationic poly(ethylene imine)-covered glass, while no adhesion of those shells on uncoated glass is found. The adhering shells are deformed and obtain a truncated sphere topology with a circular adhesion disk. The radius of the adhesion disks can reach up to 50% of the shell radius for shells of several tens of microns. The dependency of the size of adhesion areas on the capsule radius and capsule wall thickness is also investigated. Remarkably, the size of the adhesion areas is found to depend strongly on the wall thickness, which offers interesting perspectives for controlling capsule adhesion properties. A model based on the energy balance of deformation and wetting energies is presented that explains the observed trends.

DOI: 10.1103/PhysRevE.69.031802 PACS number(s): 61.41.+e, 82.35.Gh, 46.25.−y, 68.35.Np

## I. INTRODUCTION

In recent years, the importance of microcapsule systems for life-science applications in fields as diverse as medicine, cosmetics, or food design has continuously increased. Generally, microcapsules are used to encapsulate agents in order to have better control over release rates, which can either mean to achieve a slower and more continuous release or even, in the case of medical applications, to have targeted release in certain parts of the body only. In most of the applications mentioned here, the adhesion of microcapsules onto surfaces is essential for their function. Still, from a basic science point of view, the understanding of this process is poor. The aim of this paper is to shed light on a particular aspect of the adhesion process, the impact of the capsules' compliance on the size of adhesion areas.

Polyelectrolyte multilayer capsules that were introduced by Donath *et al.* [1] are an ideal model system for studying microcapsule adhesion, since they can be produced with a well-defined radius, wall thickness, and surface energy and all of those parameters can be varied over orders of magnitude. The capsules are made in a two-step process. In the first step, charged colloidal template particles are coated using the layer-by-layer electrostatic self-assembly method that was first introduced by Decher [2]. A recent review of the field can be found in [3]. In the second step, the template particles are dissolved under conditions that are not destroying the multilayer [1]. Provided the dissolution products can permeate the multilayer, capsules with walls determined by the original particle coating remain after the dissolution procedure.

In previous studies, it has been shown that the thickness of the multilayers and thus of the capsule walls is linear in the number of deposition steps, and single polyelectrolyte layers can have thicknesses in the nanometer range [4]. As well, the wetting properties are determined by the last adsorbed layer, as shown by contact angle measurements [5,6] and (indirectly) by electrophoretic measurements on coated colloids [7] and coated flat surfaces [8]. For recent reviews on hollow polyelectrolyte shells, see [9,10]. We limit ourselves here to investigating shells made from poly(allylamine hydrochloride) (PAH) and poly(sodium 4-styrenesulfonate) (PSS) since this system is the best characterized polyelectrolyte multilayer (PEM) system (see [11] for an overview).

We present here direct measurements of the size of adhesion areas of PEM shells on flat oppositely charged substrates using reflection interference contrast microscopy [12,13] and fluorescence microscopy. It is found that shells adhering to solid substrates are significantly deformed due to their adhesive interactions leading to circular contact disks in the range of several microns diameter for shells of 10–30 $\mu$m diameter. The dependency of the adhesion area radius on the shell radius and wall thickness is investigated. We discuss the observed dependences in terms of a simple model that is based on the balance of surface interactions and mechanical deformation energies.

## II. EXPERIMENT

Poly(sodium 4-styrenesulfonate) (PSS, $M_w = 70\,000$ g/mol), poly(allylamine hydrochloride) (PAH, $M_w = 70\,000$ g/mol), and poly(ethylene imine) (PEI, branched, $M_w = 25\,000$ g/mol) were purchased from Aldrich. Rhodamine B isothiocyanate was purchased from Fluka. Poly(D, L lactide) (PLA, $M_w = 20\,000$ g/mol) was obtained from Boehringer Ingelheim. Dispersions of polystyrene latex particles with a diameter of 21.1 ($\pm 0.34$) $\mu$m (monodisperse, 10% in volume fraction) were purchased from microparticles GmbH (Berlin).

All chemicals were used without further purification except for the PSS, which was dialyzed against water ($M_w$ cutoff 14 000 g/mol) and lyophilized prior to use. For all experiments and for all cleaning steps, deionized water from a Purelab Plus UV/UF system (Elga LabWater GmbH) with a conductivity of 0.055 $\mu$S cm$^{-1}$ was used.

Rhodamine B isothiocyanate labeled PAH (RBITC-PAH)

*Author to whom correspondence should be addressed. Email address: andreas.fery@mpikg-golm.mpg.de

 

was prepared as described in [14]. PLA particles with a radius between 5 and 25 $\mu$m were fabricated according to [15].

The capsules were prepared according to [16], except that the concentration of the PSS was 2 mg/mL. The shells prepared in this study had different thicknesses measured by SFM as reported in Sec. IV. In all cases, PSS was used as a last layer, rendering the shells negatively charged.

The particles were dissolved with tetrahydrofurane (THF) by washing the coated particles at least three times with THF and afterwards three times with water to remove all the particle material and the THF, respectively.

The coverslips were cleaned by the RCA method [17] prior to the PEI coating. For the coating, a drop of aqueous PEI solution (3 mg/mL) was brought onto the glass. After ten minutes, it was washed off and the glass was dried with a nitrogen stream. The coverslips were used immediately after coating.

## III. METHODS

The completeness of particle removal and the thickness of the capsule walls were determined by AFM imaging of capsules dried on mica, using a Multimode Nanoscope IIIA AFM (Veeco Instruments GmbH, Unterschleißheim) in Tapping mode. Tapping mode silicon cantilevers (Nanosensors NCH-W, NanoWorld Services GmbH, Erlangen) with a nominal spring constant of 31–50 $\mathrm{N\,m^{-1}}$ and resonance frequency of 302–350 kHz were used.

The optical microscope was a Zeiss Axiovert 200 (Zeiss, Germany), which was used both in reflection interference contrast (RICM) and fluorescence mode. In RICM, the sample is illuminated with monochromatic light in reflection geometry [12,13]. Depending on the local distance between the capsule wall and the glass surface, the reflected light is interfering constructively or destructively. From the resulting interference pattern, the shape of the capsule can be reconstructed using the method described in [18]. An Hg-vapor lamp with a monochromator (576 nm) served as the light source. A Zeiss Antiflex 63XNO 1.25 oil-immersion objective with suitable polarizers was used to avoid internal reflections. The images were recorded with a Zeiss AxiocamHR high-resolution monochromatic camera. The microscope setup could be easily switched between fluorescence and RICM mode during the experiment, because the monochromatic wavelength for the RICM was chosen identical to the excitation wavelength of the rhodamine dye. In the experiment, a few microliters of the solution containing the shells were deposited onto a thin glass slide. Fluorescence microscopy was used to determine the radii of the shells and to control the overall capsule shape prior to the measurement in order to sort out capsules that were deformed or otherwise damaged (about 30%). The adhesion areas of the capsules were monitored with RICM.

## IV. RESULTS

In Fig. 1, an image of a dried shell on mica is shown. A statistical height analysis of the images can be done after background corrections by flattening or by line fits, to give the surface of the substrate as a first maximum in the height distribution histogram. Later maxima correspond to twice or higher orders of two times the shell thickness.

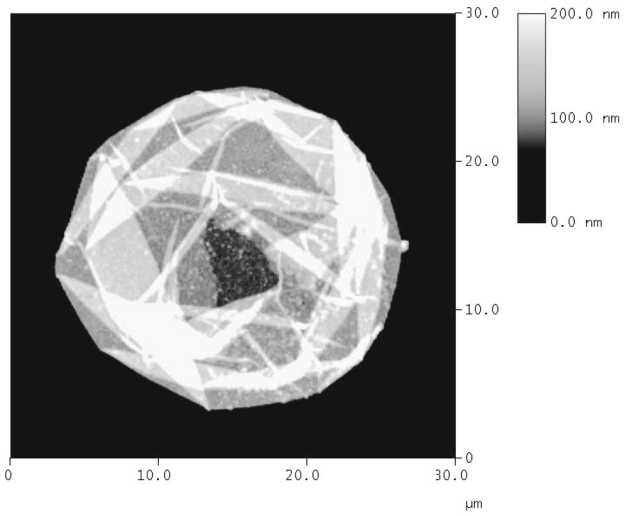


FIG. 1. AFM image of a dried shell on mica. The drying process results in a collapse of the capsule, which shows a folded flat topography.

The thicknesses scale linearly with the number of layers. This analysis resulted in an average thickness of one double layer of 4.2 nm for the shells from the PLA templates and of 4.6 nm for the shells from the PS templates. The scattering of the values was about 10%. The thickness values thus determined are within the range reported in the literature for this system (between 2.6 nm [19] and 10 nm [20], depending on the details of preparation). Later, the average values for the thicknesses in each batch are used.

The radii of the shells from the PS templates were always around 10.5 $\mu$m, which is identical to the radius of the template particles. For shells made from the polydisperse PLA templates, the size distribution before and after remained the same.

Therefore, it can be assumed that if any swelling during the dissolution of the particle had occurred [21], it is at least reversible. The equatorial radius of the shells did also not change after the adhesion.

## V. ADHESION EXPERIMENTS

### A. Qualitative description

Adhesion experiments were carried out by depositing a droplet of water containing the negatively charged shells onto the PEI-coated glass slides. After a few minutes, the shells sedimented and started to touch the glass surface. Upon touching, the shells were found to stick to the PEI-coated glass, while control experiments on cleaned noncoated glass showed no sticking but Brownian motion of the shells.

For this system, the dominating role of the electrostatic (double layer) interactions under our conditions has been shown by Zeta-potential measurements [4,22] and surface forces apparatus measurements [23] in which quantitative

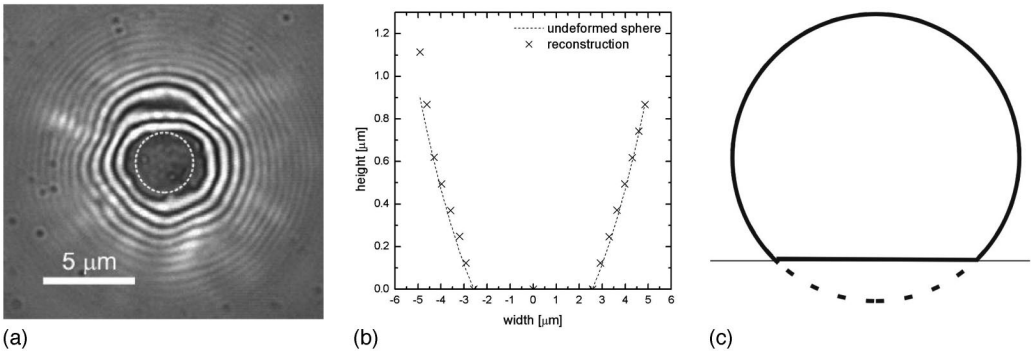


FIG. 2. (a) A typical RICM image of an adhering shell, (b) the corresponding shape reconstruction, and (c) a sketch of the truncated sphere geometry.

agreement of the long-range forces with DLVO theory predictions was shown. Finally, we also have carried out colloidal probe atomic force microscopy measurements [24], which also show quantitative agreement of long-range interactions with DLVO and pH sensitivity of the adhesion force that can be explained by the dependency of the degree of dissociation of the involved polyelectrolytes on pH. Thus, it can be assumed that electrostatic interactions are responsible for the observed adhesion.

Figure 2(a) shows a typical RICM image of an adhering shell. The adhesion area can be seen as a gray area in reflected light, which becomes darker with increasing thickness. Figure 2(b) shows the corresponding shape reconstruction using the method described in [18] in comparison to a truncated sphere fit using the shell radius that was obtained from fluorescence microscopy measurements of the equatorial diameter of the shell. Good agreement between the data and the fit is found, which suggests that the shells are adhering in truncated sphere geometry as sketched in Fig. 2(c). Deviations from the ideal cases are discussed below.

The shape of the shells' contact area on the substrate is usually circular. About 30% of the shells were not taken into account in the evaluation, since they showed strong deviations from the spherical shape (indentations) most likely due to mechanical stresses during the preparations prior to the adhesion process. For large adhesion areas, deviations from the circular shape of the adhesion areas are getting increasingly more important. Nevertheless, the difference between the radius of the circumference and the radius of the biggest circle fitting completely into the adhesion zone [see Fig. 2(a)] remained smaller than 20% in all cases. The intermediate of those two radii was taken as the adhesion radius.

The adhesion areas are not homogeneously colored, but show some variation in gray scale, which indicates that the membrane is not adhering perfectly flat to the substrate but that there is a microscopic corrugation of the contact area. For one batch of shells, buckling in the contact areas was found (see Fig. 6), which will be discussed in detail below, and those capsules were not taken into account for evaluation of the adhesion areas. In the following, the radius of the adhesion area as indicated in Fig. 2(a) is used as a measure of the extent of shell deformation due to the adhesion forces and to calculate the apparent contact area. However, as explained below, care must be taken since the microscopic contact area is lower than the apparent contact area that is calculated based on this radius.

In order to determine the dependency of the adhesion radius on the radius of the shells made from the PLA templates, we took a polydisperse sample of the shells and brought them onto a PEI-coated coverslip. Then, the radius of the adhesion area and the radius of the shell were measured for each shell. The result for a constant wall thickness of 25.4 nm is shown in Fig. 3.

As one can see clearly, the radius of the adhesion area increases with increasing shell radius. The scattering of the data is due to different reasons. First, it can be attributed to the scattering in the shell thicknesses. Secondly, it may also be due to deviations of the adhesion area from the spherical shape as discussed above. The fits to the data will be explained below.

After varying the size of the shells, the influence of the thickness of the shells has been studied by taking shells from the monodisperse PS templates of four different wall thick-

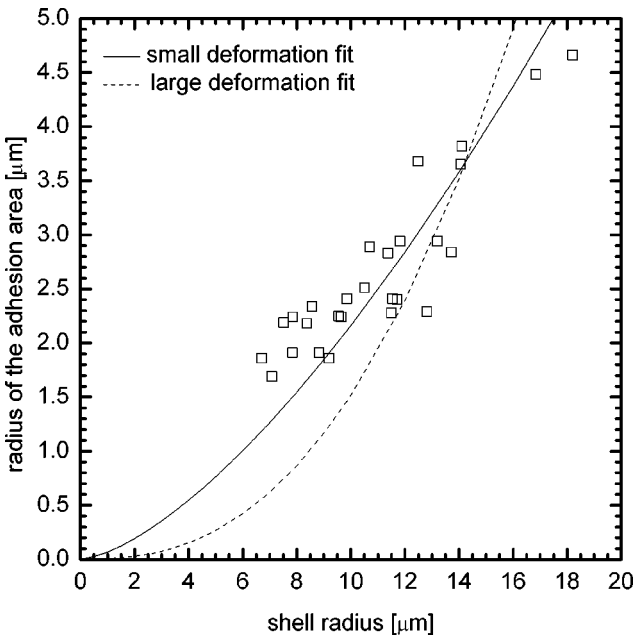


FIG. 3. The radius of the adhesion area plotted vs the radius of the shells for 25.4-nm thickness (12 layers of PAH/PSS) on a PEI-coated coverslip.

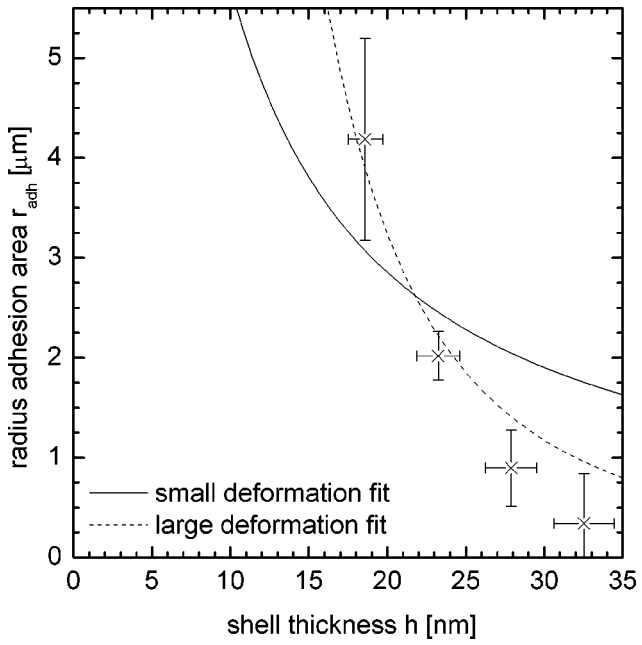


FIG. 4. Plot of the adhesion areas vs the shell thickness for monodisperse 10-$\mu$m shells. The adhesion area of the 33-nm-thick shells shown in the diagram just indicates the upper limit for the adhesion area.

nesses and measuring the adhesion area (Fig. 4).

Each point represents the average adhesion area of at least ten shells. The adhesion area increases with decreasing shell thickness, since the shell becomes more flexible, as will be discussed in detail below. For the 19-nm-thick shells, adhesion radii of up to half the shell radii could be found, whereas the adhesion area for most of the 33-nm-thick shells was not detectable. However, these shells were still adhering to the surface, which could be seen by their deformation, as well as by the fact that they were not moving in Brownian motion. The broken and full lines are theoretical predictions that will be discussed in the following.

## VI. DISCUSSION

In general, the size of the contact area of colloidal particles on adhesive surfaces is governed by the balance of energy costs for the mechanical deformations that are necessary for establishing the contact zone and the energy gain due to the work of adhesion. Since in our case adhesion areas have dimensions of several microns, the energy gain $E_{\mathrm{adh}}$ due to establishing the capsule-substrate contact can be described by a simple contact potential approach,

$$E_{\mathrm{adh}} = \pi R_{\mathrm{adh}}^2 \gamma,$$

where $R_{\mathrm{adh}}$ is the radius of the contact disk and $\gamma$ is the (negative) energy gain per contact area. For the case of a truncated sphere of radius $R$ and indentation $\Delta$ [see Fig. 2(c)], this can be written as

$$E_{\mathrm{adh}} = 2\pi R \Delta \gamma$$

for $R \gg \Delta$.

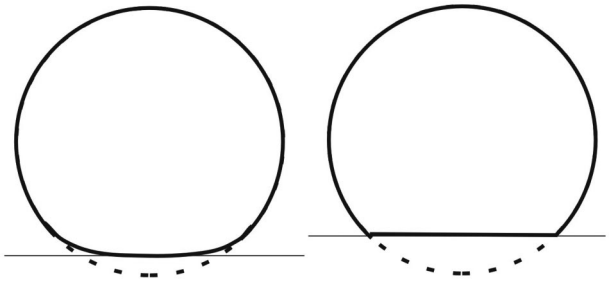

FIG. 5. Shell in weak and strong deformation regime.

In order to establish a contact area, the microcapsule has to deform, as is sketched in Fig. 2(c), and this deformation is accompanied by an energy cost $E_{\mathrm{def}}$. The first important point here is that the PEM shells are highly permeable to the solvent and also for low molecular weight molecules on the time scale of the measurement (which is several minutes up to 1 h) [25]. In contrast to the case of vesicles or cells, the volume enclosed in the capsule is not kept constant by osmotic pressure. In other words, there are no membrane tensions due to volume constraint. Consequently, in terms of energy cost for the deformation, the shells can be treated as ''empty.''

The problem of a force acting on an elastic shell of a given thickness can be treated using a continuum mechanics approach [26–28]. Qualitatively, there are two different regimes of deformation. As sketched in Fig. 5, for weak forces, the deformation remains local, upon reaching a critical force, the shell buckles, and the main energy contribution now stems from the ringlike region in which the curvature of the shell is reversed. Although in our situation the additional adhesion forces acting can prevent the buckling, the main deformation in this case is still located in the ringlike region of strong bending such that the buckled shell can serve as an approximation for the adhering shell case [29,30].

For both scenarios, the deformation energy can be written in an analytical form (a proportionality constant that is of the order of 1 containing the Poisson number of the wall material is omitted for simplicity),

$$E_{\mathrm{def,small}} \approx \frac{E h^2}{\sqrt{12R}} \Delta^2,$$

$$E_{\mathrm{def,large}} \approx \frac{E h^{5/2}}{12^{3/4} R} \Delta^{3/2}.$$

Here $E$ denotes the Young modulus of the wall material, $h$ the wall thickness, $R$ the radius of the shell, and $\Delta$ the indentation. From the extent of the deformations that are occurring in the system, it is not straightforward to decide which theory has to be applied, since one is close to the transition point between the weak and strong deformation regime. Therefore, both cases will be considered in the following.

As a result of both surface forces and mechanical properties, the indentation $\Delta$ will adjust such that the total energy of the system is minimal. Thus, the equation

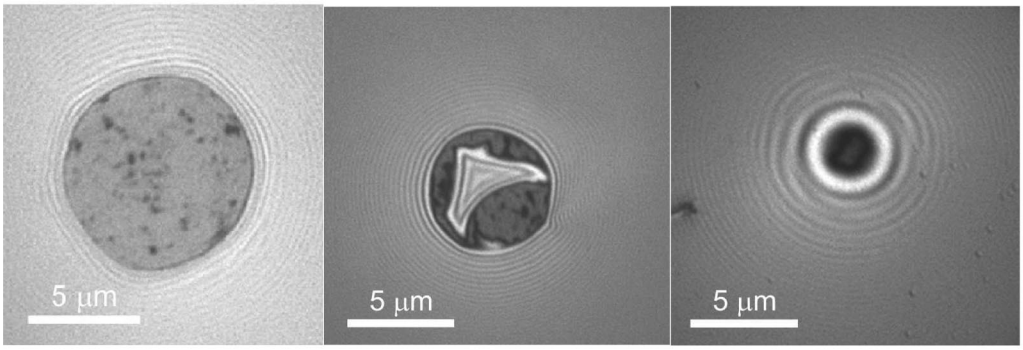


FIG. 6. Typical RICM pictures of adhering shells of 8, 10, and 14 layers wall thickness. Whereas the 8-layer shell exhibits a round and homogeneous adhesion area, the 10-layer shell already starts to buckle, which can be seen by the discontinuous adhesion area. The adhesion area of the other 14-layer shell is hardly detectable. The black area and the white fringes indicate the strong deformation.

$$\frac{\partial}{\partial \Delta}(E_{\mathrm{adh}}+E_{\mathrm{def}})=0$$

allows us to resolve for the indentation $\Delta$. Using again the geometrical relation $R_{\mathrm{adh}} \approx \sqrt{2R\Delta}$ for the adhesion radius, one finds for the small and large deformation the following expressions:

$$R_{\mathrm{adh,small}}=\sqrt{\frac{2\sqrt{12}\pi R^3\gamma}{Eh^2}},$$

$$R_{\mathrm{adh,large}}=\sqrt{2R}\left(\frac{4\times 12^{3/4}\pi R^2\gamma}{3Eh^{5/2}}\right).$$

The radius $R$ and the thickness $h$ have been measured as described in Sec. IV. The Young modulus of the shell material has been independently determined by Gao [31,32] and by us [33] to be in the range of 1.5–2 GPa. Thus, the only unknown parameter is the adhesion energy. Fitting the radius dependency in Fig. 3, we find that the small deformation model agrees better with the experimental data, while it is not reproducing the pronounced thickness effect that is found in the thickness dependency (Fig. 4). Here, the strong deformation model is in better agreement. Looking at the absolute values of the adhesion energy, we find for the small deformation model $\gamma=0.28\pm0.02\ \mathrm{mJ\,m^{-2}}$ from the radius and $0.26\pm0.07\ \mathrm{mJ\,m^{-2}}$ from the thickness dependency fit. The strong deformation model yields $0.026\pm0.002$ and $0.027\pm0.003\ \mathrm{mJ\,m^{-2}}$, respectively. These values are of the same order of magnitude as found in [34]. We have done independent measurements [24] using colloidal probe AFM to estimate the adhesion energies between PSS-terminated multilayers and PAH-terminated multilayers from pull-off forces, which yielded adhesion energies between 0.2 and 0.5 $\mathrm{mJ\,m^{-2}}$.

In all of those cases, it has to be considered that these values of $\gamma$ are effective surface energies that depend on the roughness of the surfaces [35]. In the case of rough surfaces adhering to each other, the contact area is decreased due to the microscopic corrugations. The variation in gray scale in the RICM images of the contact areas that we have found (as discussed in Sec. II) is direct evidence of these microscopic deviations from the perfectly flat contact. Thus, since we have calculated the adhesion energies assuming a flat contact, these adhesion energies are effective adhesion energies and a flat contact of the same surfaces would yield higher adhesion energies.

Viewing the facts that surface energies obtained from both models from radius and thickness dependency are matching and that as well the absolute value obtained from the small deformation model is the same as the one obtained by an independent method, the small deformation model seems clearly to better account for the data. However, regarding the shape of the adhesion zones for the different thicknesses, this picture is questioned, as can be seen in Fig. 6.

For eight layers, a flat adhesion area terminated by a rim in which the shell is strongly bent is clearly visible and thus the large deformation model should be applicable (see the sketch in Fig. 5). The gradual flattening predicted for small deformations is found only for the adhesion areas for 14 layers where a flat adhesion area is not detectable with the resolution of the setup (0.5 $\mu$m), so in this case the small deformation model should be applicable. The 10-layer shells show a special behavior, since in this case some of the contact areas were not flat, but showed large dimples with polygon-shaped edges. This could be interpreted as a transition state from adhesion-induced small deformations to large deformations. Therefore, the large deformation model describes the behavior of the thin shells and the small deformation model describes the behavior of thick shells better. Studies using finite-element analysis to treat the deformation problem are on the way.

The main shortcoming of the model is that friction between the capsule and the substrate is neglected. Due to entanglements, however, it is to be expected that the capsule and the surface cannot slide without friction, which would give rise to additional stretching and thus additional energy cost for the deformations. The mechanical cost of the folds within the contact area is neglected as well. Both simplifications result in an underestimation of the energy necessary to deform the shell, which is reflected in the low apparent interaction energies. It cannot be excluded that in extreme cases the PEI layer desorbs from the glass surface.

## VII. CONCLUSION AND SUMMARY

We have investigated the adhesion of hollow shells of defined thickness made from polyelectrolyte multilayers to flat substrates. Adhesion can be triggered by electrostatic interactions and we have focused on the adhesion of negatively charged capsules to positively charged substrates. We find that shells are adhering in truncated sphere geometry and we could measure the radius of the contact disk for shells between 5 and 50 $\mu$m. Both the radius and the thickness of the shells were varied while the surface properties of the shells were not changed and the size of the adhesion areas was monitored as a function of those parameters. Using a simple energy minimization, the dependency could be explained by the competition of mechanical deformation energies and adhesion energies. The mechanical deformation energies of the shells were described using Landau theory for elastic shells. It is possible to predict the scaling of the adhesion radius $R_{\mathrm{adh}}$ with shell thickness $h$ and radius $R$ depending on the deformation model employed, being proportional to $(R/h)^{5/2}$ for the large and to $(R^{3/2}/h)$ for the small adhesion model. An important finding is the strong dependency of the adhesion area on the shell thickness, since this opens interesting perspectives for control of the adhesive properties. Rather than changing the wetting properties of shells to increase or decrease adhesion, one can design shells to have a certain adhesion strength simply by controlling their dimensions, in particular the thickness and radius, as has been demonstrated here. This renders the system much more versatile than classical colloidal particles for controlling adhesion. Recent results on the mechanics of actin-decorated vesicles, where buckling behavior of the membranes is found as well [36], suggest that concepts like those described above can also be relevant for cell adhesion, although this is beyond the scope of the present study.

## ACKNOWLEDGMENTS

We would like to thank U. Schwarz and H. Möhwald for discussions and A. Heilig for shell thickness measurements. The Max Planck Society is acknowledged for financial support.

[1] E. Donath, G. B. Sukhorukov, F. Caruso, S. A. Davis, and H. Möhwald, Angew. Chem., Int. Ed. Engl. **37**, 2202 (1998).
[2] G. Decher, J. D. Hong, and J. Schmitt, Thin Solid Films **210/211**, 831 (1992).
[3] G. Decher, in *Multilayer Thin Films*, edited by J. B. Schlenoff (Wiley-VCH, Weinheim, 2003), p. 1.
[4] G. B. Sukhorukov, E. Donath, H. Lichtenfeld, E. Knippel, M. Knippel, A. Budde, and H. Möhwald, Colloids Surf., A **137**, 253 (1998).
[5] M. C. Hsieh, R. J. Farris, and T. J. McCarthy, Macromolecules **30**, 8453 (1997).
[6] W. Chen and T. J. McCarthy, Macromolecules **30**, 78 (1997).
[7] G. B. Sukhorukov, E. Donath, S. Davis, H. Lichtenfeld, F. Caruso, V. I. Popov, and H. Möhwald, Polym. Adv. Technol. **9**, 759 (1998).
[8] G. Ladam, P. Schaad, J. C. Voegel, P. Schaaf, G. Decher, and F. Cuisinier, Langmuir **16**, 1249 (2000).
[9] H. Möhwald, E. Donath, and G. Sukhorukov, in *Multilayer Thin Films*, edited by J. B. Schlenoff (Wiley-VCH, Weinheim, 2003).
[10] M. Schönhoff, Curr. Opin. Colloid Interface Sci. **8**, 86 (2003).
[11] X. Arys, A. Jonas, A. Laschewsky, and R. Legras, in *Supramolecular Polymers*, edited by A. Ciferri (Marcel Dekker, New York, 2000), p. 505.
[12] D. Gingell and I. Todd, Biophys. J. **26**, 507 (1979).
[13] J. Rädler and E. Sackmann, J. Phys. II **3**, 727 (1993).
[14] G. Ibarz, L. Dähne, E. Donath, and H. Möhwald, Adv. Mater. (Weinheim, Ger.) **13**, 1324 (2001).
[15] D. B. Shenoy, A. A. Antipov, G. B. Sukhorukov, and H. Möhwald, Biomacromolecules **4**, 265 (2003).
[16] F. Caruso, E. Donath, and H. Möhwald, J. Phys. Chem. B **102**, 2011 (1998).
[17] W. Kern and D. A. Puotinen, RCA Rev. **31**, 187 (1970).
[18] G. Wiegand, K. R. Neumaier, and E. Sackmann, Appl. Opt. **37**, 6892 (1998).
[19] S. Leporatti, A. Voigt, R. Mitlöhner, G. Sukhorukov, E. Donath, and H. Möhwald, Langmuir **16**, 4059 (2000).
[20] F. Caruso, K. Niikura, D. N. Furlong, and Y. Okahata, Langmuir **13**, 3422 (1997).
[21] C. Gao, S. Moya, H. Lichtenfeld, A. Casoli, H. Fiedler, E. Donath, and H. Möhwald, Macromol. Mater. Eng. **286**, 355 (2001).
[22] E. Donath, D. Walther, V. N. Shilov, E. Knippel, A. Budde, K. Lowack, C. A. Helm, and H. Möhwald, Langmuir **13**, 5294 (1997).
[23] K. Lowack and C. A. Helm, Macromolecules **31**, 823 (1998).
[24] V. Bosio, thesis, Universität Potsdam, 2003 (unpublished).
[25] A. A. Antipov, G. B. Sukhorukov, E. Donath, and H. Möhwald, J. Phys. Chem. B **105**, 2281 (2001).
[26] L. D. Landau and E. M. Lifschitz, *Elastizitätstheorie* (Akademie Verlag, Berlin, 1991).
[27] L. Pauchard, Y. Pomeau, and S. Rica, C. R. Acad. Sci., Ser. IIb: Mec., Phys., Chim., Astron. **324**, 411 (1997).
[28] L. Pauchard and S. Rica, Philos. Mag. B **78**, 225 (1998).
[29] U. S. Schwarz, S. Komura, and S. A. Safran, Europhys. Lett. **50**, 762 (2000).
[30] U. S. Schwarz, S. A. Safran, and S. Komura, in *Dynamics in Small Confining Systems V*, edited by J. M. Drake, J. Klafter, P. Levitz, R. M. Overney, and M. Urbakh, MRS Symposia Proceedings No. 651 (Materials Research Society, Pittsburgh, 2001), p. T5.3.1.
[31] C. Gao, S. Leporatti, S. Moya, E. Donath, and H. Möhwald, Langmuir **17**, 3491 (2001).
[32] C. Gao, E. Donath, S. Moya, V. Dudnik, and H. Möhwald, Eur. Phys. J. E **5**, 21 (2001).
[33] F. Dubreuil, N. Elsner, and A. Fery, Eur. Phys. J. E **12**, 215 (2003).
[34] K. K. Liu, V. Chan, and Z. Zhang, Med. Biol. Eng. Comput. **40**, 491 (2002).
[35] B. N. J. Persson, Eur. Phys. J. E **8**, 385 (2002).
[36] E. Helfer, S. Harlepp, L. Bourdieu, J. Robert, F. C. MacKintosh, and D. Chatenay, Phys. Rev. Lett. **87**, 088103 (2001).